Magn Reson Med Sci 2018; 17; 283–292
doi:10.2463/mrms.mp.2017-0134
Published Online: January 15, 2018

MAJOR PAPER

Differentiating between Alzheimer Disease Patients and Controls with Phase-difference-enhanced Imaging at 3T: A Feasibility Study

Machiko Tateishi[1], Mika Kitajima[1*], Toshinori Hirai[2], Tetsuya Yoneda[3], Mamoru Hashimoto[4], Nan Kurehana[1], Hiroyuki Uetani[1], Ryuji Fukuhara[4], Minako Azuma[2], and Yasuyuki Yamashita[1]

Purpose: To test the feasibility of the phase difference enhanced (PADRE) imaging for differentiation between Alzheimer disease (AD) patients and control subjects on 3T MR imaging.

Materials and Methods: Fifteen patients with AD and 10 age-matched control subjects underwent two-dimensional fast field echo imaging to obtain PADRE images on a 3T MR scanner. A double Gaussian distribution model was used to determine the threshold phase value for differentiation between the physiologic and non-physiologic iron in the cerebral cortices, and PADRE images were processed with the threshold. Using a 4-point grading system, two readers independently assessed the signal of the four cerebral cortices on PADRE images: the cuneus, precuneus, superior frontal gyrus, and superior temporal gyrus. The difference in the signals in each cortex between the AD patients and age-matched control subjects was determined by using Mann–Whitney U test. Inter-rater reliability was determined by Kappa analysis. We also evaluated the correlation between Mini-Mental State Examination (MMSE) score and the hypointense grade, and between disease duration and the hypointense grade using the Spearman rank correlation test.

Results: The threshold phase value for differentiation between the physiologic and non-physiologic iron was −4.6% π (radian). The mean grades of the cuneus, precuneus, and superior temporal gyrus were significantly higher for the AD patients than for the control subjects ($P = 0.002$). Excellent inter-rater reliability was seen in the precuneus (kappa = 0.93), superior temporal gyrus (kappa = 0.94), and superior frontal gyrus (kappa = 0.93); good inter-rater reliability was observed in the cuneus (kappa = 0.75). We found a statistical correlation between MMSE score and the hypointense grade in superior temporal gyrus (STG) ($P = 0.008$), and no correlation between disease duration and the hypointense grade in any gyrus.

Conclusion: Our results suggest the feasibility of PADRE imaging at 3T for differentiation between AD patients and control subjects.

Keywords: *Alzheimer disease, phase difference enhanced imaging, 3T magnetic resonance*

Introduction

Alzheimer's disease (AD) is the most common primary neurodegenerative disease presenting dementia. Neuritic plaques comprised of amyloid-β (Aβ) and neurofibrillary tangles are the pathological hallmarks of AD,[1] Aβ accumulates in the preclinical stage of AD. Treatment strategies using disease-modifying drugs potentially could be extended at the prodromal stage in the near future. Therefore, early diagnosis of AD is important for appropriate treatment and management. A diagnostic problem in AD is that there are currently no methods to demonstrate amyloid deposition *in vivo* except for positron emission tomography (PET) in combination with ^{11}C-labeled Pittsburgh compound-B (^{11}C-PIB), ^{18}F-florbetapir, florbetaben, and flutemetamol. However, the need to use ionizing radiation, relatively high costs, and limited availability of PET systems limit the use of PET clinically.[2–4] In an ultrahigh-field 7T MR imaging study,[5] the susceptibility changes of the cerebral cortex differed between AD patients and normal control subjects. However, the availability of 7T MR systems is very limited in clinical practice.

[1]Department of Diagnostic Radiology, Faculty of Life Sciences, Kumamoto University, 1-1-1 Honjo, Chuo-ku, Kumamoto, Kumamoto 860-8556, Japan
[2]Department of Radiology, Faculty of Medicine, University of Miyazaki, Miyazaki, Japan
[3]Department of Medical Physics in Advanced Biomedical Sciences, Faculty of Life Sciences, Kumamoto University, Kumamoto, Japan
[4]Department of Neuropsychiatry, Faculty of Life Sciences, Kumamoto University, Kumamoto, Japan
*Corresponding author, Phone: +81-96-373-5261, Fax: +81-96-362-4330, E-mail: mkitaji@kumamoto-u.ac.jp

Received: September 12, 2017 | Accepted: December 8, 2017

There are several MR imaging techniques using phase information.[6–8] The susceptibility-weighted imaging, which uses a negative phase, demonstrates excellent image contrast and reveals anatomical structures, that are not visible on conventional MR images.[7] The quantitative susceptibility mapping (QSM) can quantify the susceptibility.[8] In contrast, phase difference-enhanced (PADRE) imaging can use any phases and the phase difference between the target and surrounding tissue is enhanced.[9,10] PADRE can delineate fine anatomical structures that are not well resolved on conventional MR images[9–11] and detect early pathological changes in several types of neurodegenerative diseases on 3T MRI.[10]

This PADRE technique has been applied for detection of amyloid-related iron in an animal study using an AD transgenic mouse on 7T MRI that showed hypointense foci in the cerebral cortex on PADRE.[12] Those hypointense foci were identical to the distribution of Aβ.[12] However, the feasibility of this technique at 3T for AD patients has not been investigated. The purpose of this study was to test the feasibility of PADRE imaging for differentiation between AD patients and control subjects on 3T MRI.

Materials and Methods

The present study was approved by our institutional review board. Given its retrospective nature, written informed consent was waived.

Subjects

This study included 15 patients (5 male and 10 female patients; age range, 53–80 years; mean age, 64.1 years) who were clinically diagnosed as AD by expert psychiatrists (blinded to the results of MR imaging) according to diagnostic criteria recommended by the National Institute of Neurologic and Communicative Disorders and Stroke-Alzheimer's Disease and Related Disorders Association[13] and 10 age-matched volunteers (5 males, 5 females; age range, 51–76 years; mean age, 64.0 years). The Mini-Mental State Examination (MMSE) scores of the AD patients varied from 8 to 23 (mean, 18.5), and the disease duration varied from one to 6 years (mean 3.4 years). The control subjects were selected from the consecutive patients who had been referred from the neurology and psychiatry departments of our institution for screening of intracranial organic lesions. The criteria for the control subjects in this study were normal findings at neurologic examination, no history of neurologic disease, and normal results of brain MR imaging. We did not evaluate the cognitive function of the control subjects by the objective test such as MMSE score; however, we interviewed the participants or attending doctors, or reviewing the medical chart, and confirmed that there were no control subjects with the loss of the intellectual abilities of sufficient severity to interfere with social or occupational function.

MR imaging protocol

MR imaging was performed on a 3T system (Achieva 3.0-T; Philips Healthcare, Best, the Netherlands) with an 8-channel head coil. Two-dimensional (2D) fast field echo (FFE) MR imaging was performed in the axial plane parallel to the anterior commissure - posterior comissure (AC–PC) line with the following parameters: 890 ms/35.0 ms/50°/1 (TR/TE/flip angle/NSA, respectively), 23-cm FOV, 400 × 320 matrix, 2-mm slice thickness. The scan time was 3 min 51 s.

Optimization of PADRE imaging to enhance phase difference of cerebral cortices between AD patients and control subjects

One of the major concepts responsible for the PADRE technique is "phase difference selection," which enhances the magnetic properties of the target tissue.[9–12] To enhance the phase difference of the cerebral cortices between the AD patients and control subjects, we used the double Gaussian distribution model (Appendix).[12] In this model, we assumed that the phase of the cerebral cortices can be classified into two components of iron: physiologic iron, including age-related iron, and non-physiologic iron, including amyloid-related iron (Fig. 1). Based on the central limit theorem, the phase distribution of the two components of iron may show different Gaussian distributions. Using transgenic APP23 mice, this theory has been previously validated by comparing PADRE images with histological amyloid staining of the brain.[12] The processing method of PADRE using the double Gaussian distribution model is described in Appendix.

In this study, one medical physicist measured the phase values of the cerebral cortices on the phase images by placing multiple ROIs on the cerebral cortices in the four gyri: the cuneus (Cn), precuneus (PrCn), superior frontal gyrus (SFG), and superior temporal gyrus (STG). Attempts were made to select ROIs of approximately 30 mm^2. Their sizes were chosen to obtain ROIs large enough not to be affected by pixel variability and small enough to avoid the superficial veins running along the brain surface and subcortical U-fibers. We fit the Gaussian curve to the phase value histogram comprising sum of the phase values of the ROIs in all subjects in AD and control group using gnuplot (version 5.0, Geeknet, Inc., Sacramento, CA, USA; http://www.gnuplot.info/download.html) (Fig. 1). Then, the histogram was divided into two Gaussian curves based on the double Gaussian component model. Finally, we determined the threshold, defined as the phase value of the intersection of the two Gaussian curves on the phase value histogram, for differentiation between the physiologic and non-physiologic iron. PADRE images were reconstructed in each case by using the determined threshold.

Evaluation of PADRE Images

On PADRE images, we assessed the cerebral cortices signals of the four gyri: the Cn, PrCn, SFG, and STG. The cerebral cortices with abundant physiological iron deposition, including the primary motor cortex, visual cortex, and auditory

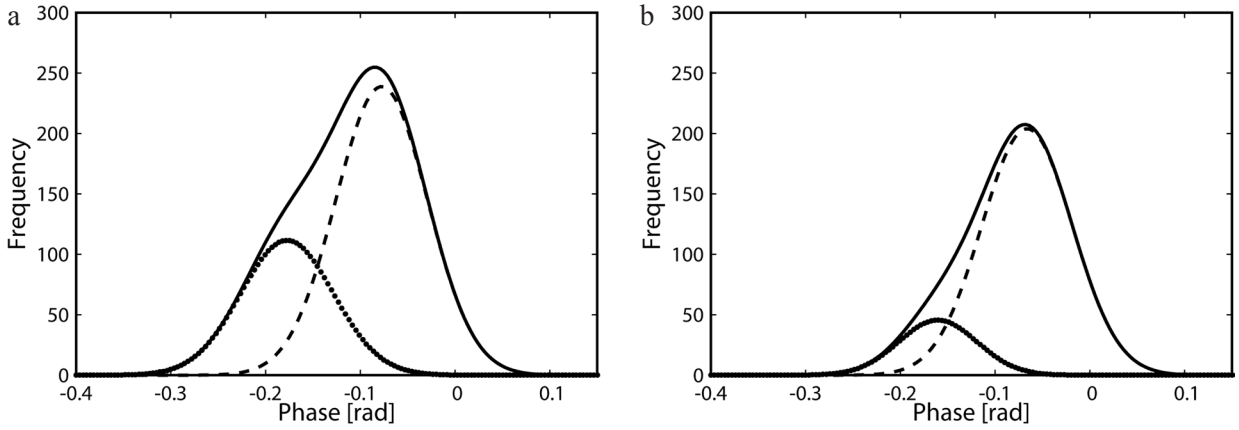

Fig. 1 Fitted original Gaussian curve comprised sum of the phase value of all ROIs and two Gaussian curves obtained based on the double Gaussian model on the phase value histogram in the Alzheimer disease (AD) patients (**a**) and control subjects (**b**). The solid line indicates the fitted curve to the frequency at each phase value in all subjects. The dashed Gaussian curve with the peak near a phase of 0 may be attributable to physiologic iron. The dotted Gaussian curve with the peak deviating to the negative phase may be attributable to non-physiological iron. In the smaller phase value than the intersection of the two Gaussian curves on the histogram, the area subtracting the area under the curve of the second curve with a lower peak height from the first curve with a higher peak height is larger in AD patients than that in controls. The intersection of the two different Gaussian curves for the AD patients was –4.6% of π (radian), and the intersection for the control subjects was –4.8% of π (radian). The phase value of the intersection of the two Gaussian curves in AD patients is used as the threshold for differentiation between the physiologic and non-physiologic iron in the processing of phase difference enhanced (PADRE) images. rad, radian.

cortex, were excluded from the evaluation, because the signal from physiological iron may affect the phases arising from non-physiological iron. We also excluded the distinct hemorrhagic foci observed as spotty low signal on T_2^*-weighed images (2D FFE images) that were the source images of PADRE. When the laterality of the cortex signal was observed, we chose the cortex with the lower signal. Because the veins running along the cortical surface were observed as low signal linear structures on the PADRE images, we carefully differentiated the cortical signal change from those veins.

Two neuroradiologists who were blinded to the patients' information, including the diagnosis of AD independently assessed the signal of the cerebral cortices of the Cn, PrCn, SFG, and STG by using a 4-point scale: grade 1, almost no hypointense foci in the cortex; grade 2, sparse distribution of hypointense foci in the cortex; grade 3, intermediate distribution of hypointense foci in the cortex; grade 4, extensive distribution of hypointense foci in the cortex (Fig. 2). The readers evaluated all the slices on which the target gyri were scanned, and the most representative signal was assigned as the grade of the evaluated gyrus. Final agreements on grading were obtained by consensus. PADRE images were presented in randomized order to the observers.

Statistical analysis

The difference in the cortical signal at the consensus readings of PADRE between the AD patients and control subjects was tested by performing the Mann–Whitney U test. Inter-rater agreement for the grade of the cortical signal was determined by the κ coefficient (κ < 0.20, poor; κ = 0.21–0.40, fair; κ = 0.40–0.60, moderate; κ = 0.61–0.80, good; κ = 0.81–0.90, very good; and κ > 0.90, excellent agreement) and the 95% confidence interval (CI).

We evaluated the correlation between the disease duration and the grade of hypointensity in each gyrus, and between MMSE score and the grade of hypointensity in each gyrus by Spearman rank correlation and the 95% CI. We also evaluated the correlation between the disease duration and the sum of hypointense grade in each AD patient, and between MMSE score and the sum of hypointense grade in each AD patient by Spearman rank correlation and the 95% CI.

A *P*-value of < 0.05 was considered as indicating a statistically significant difference for Mann–Whitney U test and Spearman rank correlation. Statistical analysis was conducted with MedCalc Statistical Software version 17.9.2 (MedCalc Software, Ostend, Belgium).

Results

In the AD patients and control subjects, the phase value histogram comprised two different Gaussian curves: the main curve with higher height, and the second curve deviating to the negative phase with lower height (Fig. 1). The intersection of the two different Gaussian curves for the AD patients was –4.6% of π (radian), and the intersection for the control subjects was –4.8% of π (radian). In the smaller phase value than the intersection of the two Gaussian curves on the histogram, the area subtracting the area under the curve of the second curve with a lower peak height from the first curve with a higher peak height is larger in AD patients than that in

Table 1 Summary of visual assessment of the four cortices

	AD patients		Control subjects		*P* value
	Number of cases (%)	Mean (SD)	Number of cases (%)	Mean (SD)	
Cn					
Grade 1	0/15 (0)		1/10 (10)		.002*
Grade 2	0/15 (0)	3.7 (0.49)	3/10 (30)	2.6 (0.84)	
Grade 3	5/15 (33.3)		5/10 (50)		
Grade 4	10/15 (66.7)		1/10 (10)		
PrCn					.002*
Grade 1	2/15 (13.3)	2.0 (0.59)	8/10 (80)	1.2 (0.42)	
Grade 2	10/15 (66.7)		2/10 (20)		
Grade 3	3/15 (20.0)		0/10 (0)		
Grade 4	0/15 (0)		0/10 (0)		
SFG					
Grade 1	7/15 (46.7)		7/10 (70)		
Grade 2	7/15 (46.7)	1.7 (0.82)	3/10 (30)	1.3 (0.48)	.243
Grade 3	0/15 (0)		0/10 (0)		
Grade 4	1/15 (6.7)		0/10 (0)		
STG					
Grade 1	1/15 (6.7)		6/10 (60)		
Grade 2	4/15 (26.7)	2.7 (0.80)	3/10 (30)	1.5 (0.71)	.002*
Grade 3	8/15 (53.3)		1/10 (10)		
Grade 4	2/15 (13.3)		0/10 (0)		

AD, Alzheimer disease; SD, standard deviation; Cn, cuneus; PrCn, precuneus; SFG, superior frontal gyrus; STG, superior temporal gyrus; *Significant difference.

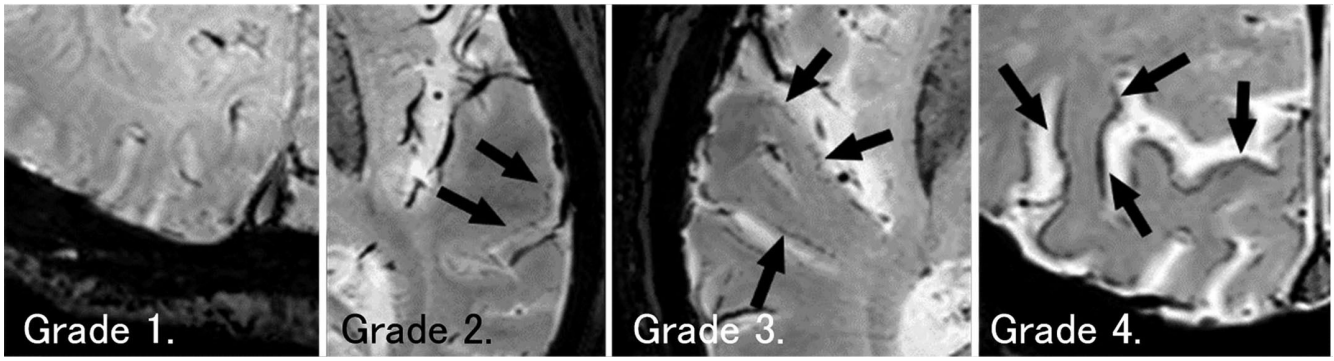

Fig. 2 Representative cases of each hypointense grade. (**Grade 1**) almost no hypointense foci in the cortex; (**Grade 2**), sparse distribution of hypointense foci in the cortex (arrows); (**Grade 3**), intermediate distribution of hypointense foci in the cortex (arrows); (**Grade 4**), extensive distribution of hypointense foci in the cortex (arrows).

controls (Fig. 1). Finally, we used a phase of −4.6% of π (radian) as the threshold for enhancement of presumed non-physiologic iron on PADRE.

The visual assessment of the four cortices is summarized in Table 1. The mean grades of the Cn, PrCn, and STG were significantly higher in the AD patients than in the control subjects ($P = 0.002$, $P = 0.002$, and $P = 0.002$, respectively) (Figs. 3 and 4). We found no statistical difference in SFG between AD patients and control subjects. Excellent inter-rater reliability was seen in the PrCn (kappa = 0.93; 95% CI, 0.81–1.00), SFG (kappa = 0.93; 95% CI, 0.78–1.00), STG (kappa = 0.94; 95% CI, 0.84–1.00). Good inter-rater reliability was observed in the Cn (kappa = 0.75; 95% CI, 0.53–0.98).

We found no correlation between the disease duration and the grade of hypointensity in AD patients (Fig. 5). For the correlation between MMSE score and the grade of hypointensity in AD patients, we found no correlation other than STG ($P = 0.008$; 95% CI, −0.873 to −0.212) (Fig. 6). In STG, MMSE score decline with advancing of the hypointensity grade; however, the variation of MMSE score was large in grades 3 and 4. Furthermore, we found no correlation between MMSE score and the sum of hypointensity grade (Fig. 6).

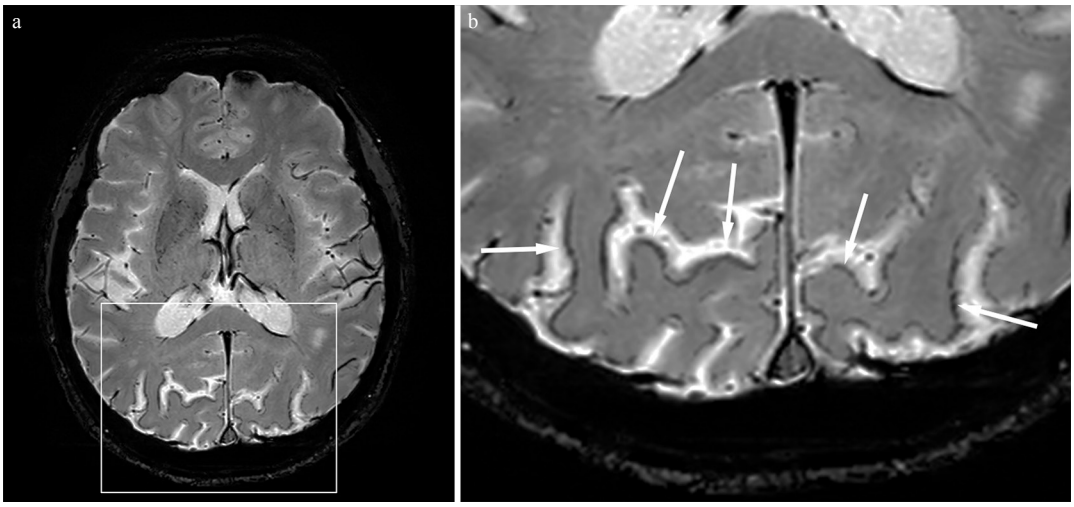

Fig. 3 A 55-year-old female with Alzheimer disease (AD). MMSE score of 19. (**a**) The hypointense foci distribute predominantly in the parietal cortex. (**b**) A magnified image of the cuneus (Cn) and precuneus (PrCn). The extensive band-like shape hypointense foci (arrows) are observed in the bilateral Cn (grade 4).

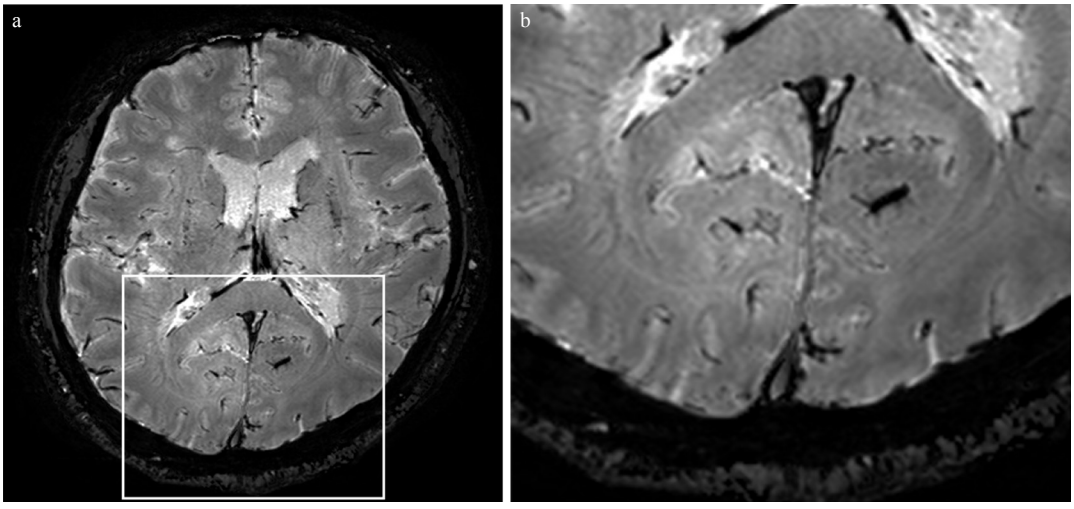

Fig. 4 A 67-year-old male control subject. (**a**) A phase difference enhanced (PADRE) image at the cuneus (Cn) and precuneus (PrCn) level. No distinct hypointense foci are observed in the cortices in this image. (**b**) A magnified image of the Cn and PrCn. No distinct hypointense foci in the Cn and PrCn (grade 1). In the superior frontal gyrus (SFG), PrCn and superior temporal gyrus (STG), there are no distinct hypointense foci.

Discussion

In our study using PADRE images acquired at 3T, there was a significant difference in the degree of hypointense foci in the specific cerebral cortices between the AD patients and control subjects. Similar to earlier studies in AD transgenic mice and human AD patients that used T_2^*-weighted 7T MR images,[5,14–17] the PADRE images showed hypointense foci in the cerebral cortices. Compared with 7T MRI, 3T MRI shows a lower signal-to-noise ratio and smaller phase changes. However, even at 3T, our pilot study demonstrated that PADRE can show signal changes in the specific cortices of AD patients within a clinically acceptable acquisition time.

In an autopsy study of AD patients,[5] amyloid deposition and neurofibrillary tangles were colocalized with iron accumulation. Therefore, hypointense foci on PADRE images in patients with AD may reflect iron accumulation. Although the animal study[12] revealed that the hypointense foci indicating iron deposition were identical to the distribution of Aβ, the histologic source of the signal change was not revealed. Iron associated with Aβ plaques can accumulate from several potential sources.[18–21] As a metalloprotein, free iron will bind to Aβ fibrils and collect within the plaques. Iron from ferritin, and its degradation to hemosiderin, can originate from nearby neurons and microglial cells that have migrated to the Aβ plaques and can become part of the plaque

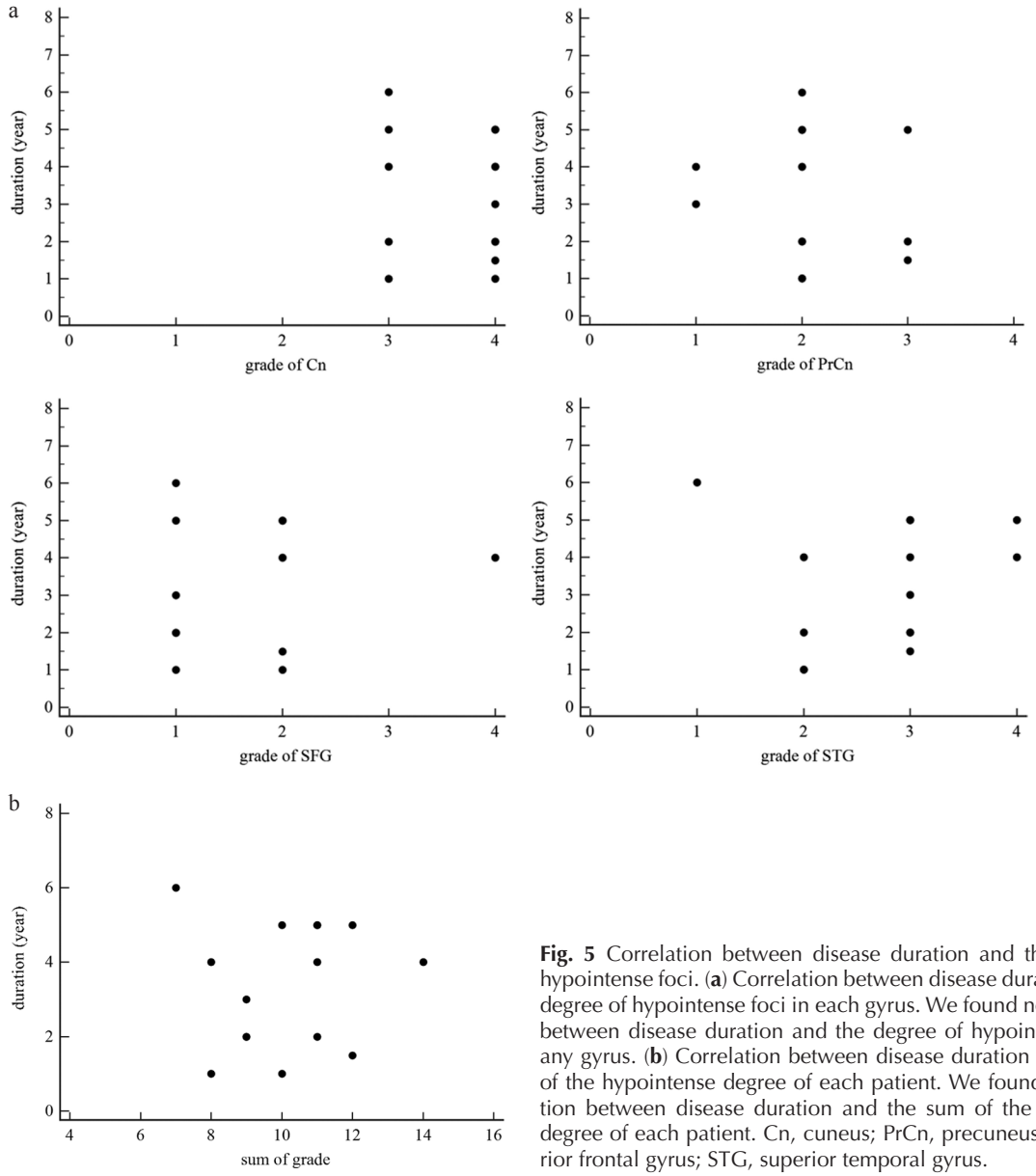

Fig. 5 Correlation between disease duration and the degree of hypointense foci. (**a**) Correlation between disease duration and the degree of hypointense foci in each gyrus. We found no correlation between disease duration and the degree of hypointense foci in any gyrus. (**b**) Correlation between disease duration and the sum of the hypointense degree of each patient. We found no correlation between disease duration and the sum of the hypointense degree of each patient. Cn, cuneus; PrCn, precuneus; SFG, superior frontal gyrus; STG, superior temporal gyrus.

mass.[18–21] In other reports, cerebral non-heme-iron accumulation is observed in post-mortem studies of healthy aging,[22] whereas several researchers have shown that hemoglobin binds to Aβ and co-localizes in amyloid plaques and cerebral amyloid angiopathy (CAA) in AD brains and hemoglobin promotes Aβ oligomer formation.[23,24] Those iron may contribute the hypointense signal on PADRE, and the difference type of iron between AD patients and control subjects may cause the phase difference. PADRE attempts to differentiate the two types of iron by weighting the specific phase value. We optimized the PADRE images conditions to enhance the cerebral cortical phase difference between AD patients and control subjects. Based on the double Gaussian model, we assumed that the phase of the cerebral cortices can be divided into two components of iron: physiological iron, including age-related iron, and non-physiological iron, including Aβ-related iron. Although the assumption was not proven by pathology in this human study, it has been validated by an animal study that used transgenic APP23 mice.[12] We think that the properties and optimization of PADRE images contributed to our results.

In early stage AD, amyloid preferentially deposits in the basal frontal, temporal, and occipital lobes. As the disease progresses, amyloid deposition extends to the parietofrontal cortex.[25] Visual inspection of PET amyloid images of AD patients have shown a typical regional brain distribution: initial deposition in the precuneus, orbitofrontal cortex, and the inferior temporal gyrus and posterior cingulate gyrus, and later by the remaining prefrontal cortex and lateral temporal and parietal cortices.[26] In our study, the SFG signal was not

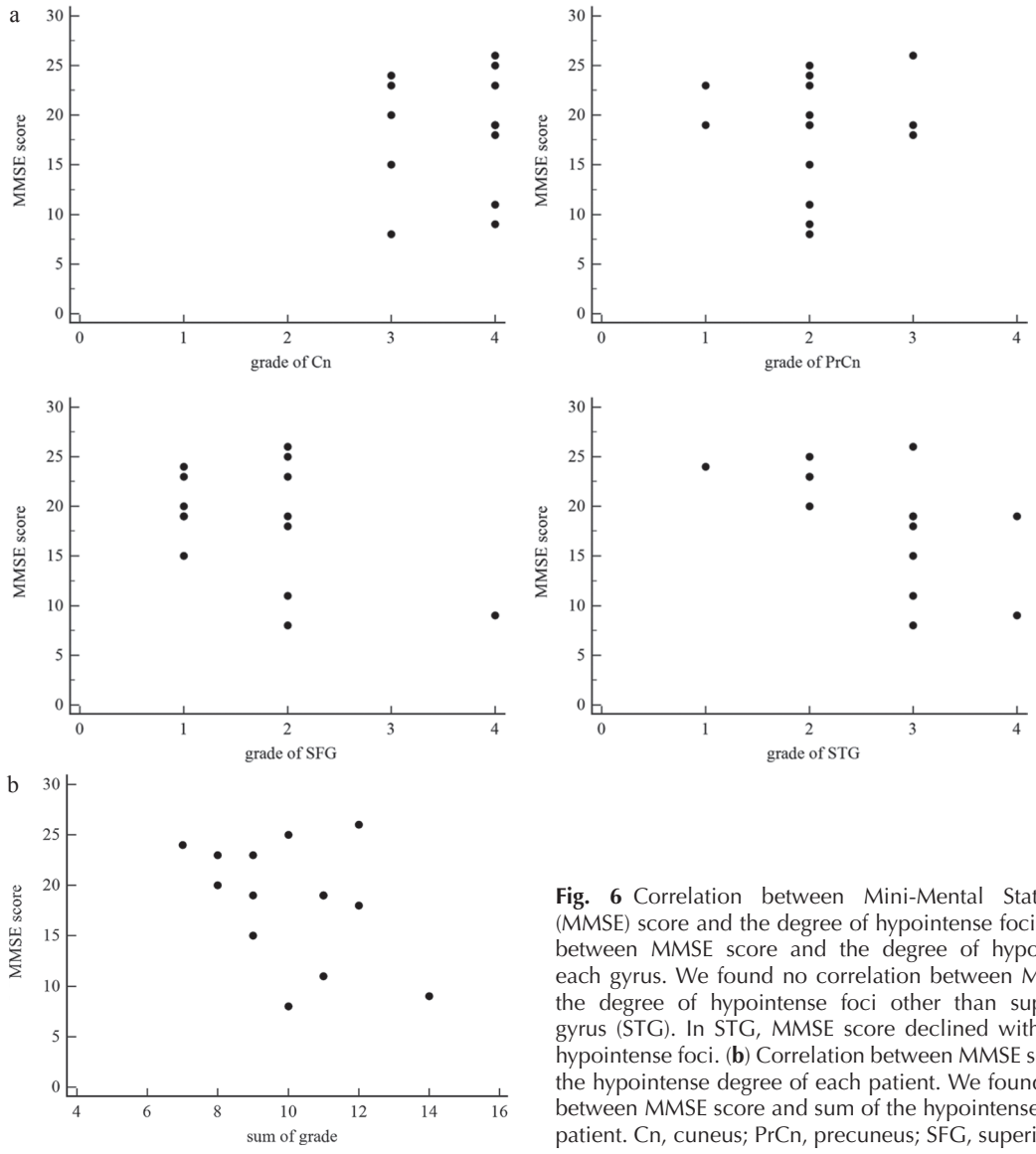

Fig. 6 Correlation between Mini-Mental State Examination (MMSE) score and the degree of hypointense foci. (**a**) Correlation between MMSE score and the degree of hypointense foci in each gyrus. We found no correlation between MMSE score and the degree of hypointense foci other than superior temporal gyrus (STG). In STG, MMSE score declined with advancing the hypointense foci. (**b**) Correlation between MMSE score and sum of the hypointense degree of each patient. We found no correlation between MMSE score and sum of the hypointense degree of each patient. Cn, cuneus; PrCn, precuneus; SFG, superior frontal gyrus.

significantly different between the AD patients and controls. Amyloid deposition may not be sufficiently high to detect on PADRE in SFG. We found no correlation between the disease duration and the hypointensity grade in any gyrus. Arnold et al.[27] reported that the distribution of neuritic plaques (Aβ plaques) was more evenly distributed throughout the cortex, with the exceptions of limbic periallocortex and allocortex, and the temporal and occipital lobes had the highest neuritic plaque densities, limbic and frontal lobes had the lowest, and parietal lobe was intermediate. Additionally, they reported that there was no relationship between the duration of illness and densities of neurofibrillary tangles or neuritic plaques. Our results consistent with the previous histologic report by Arnold et al.[27]

For the correlation between MMSE score and hypointense grade, there was a statistically correlation only in STG. However, the variation of the MMSE score was large in grade 3 and 4. Tiraboschi et al.[28] evaluated the correlation between the severity of AD evaluated with MMSE score and the density of neuritic plaques and neurofibrillary tangles in the several cortices. They showed that significant differences consistently emerged for neurofibrillary tangles (NFTs) alone across the different severity groups of AD patients. The previous study using ^{11}C-PiB PET[29] showed that Aβ deposition follows sigmoidal kinetics over time and the rates of Aβ deposition start to slow, trending towards a plateau as disease progresses. Because the patients were clinically diagnosed as AD in our study, the Aβ deposition may have reached plateau. Additionally, the small number of patients and the individual variability for the degree of Aβ deposition may affect the results. Further investigations with the sufficient number of patients and follow-up studies are required to clarify the correlation between the clinical stage of AD and PADRE findings.

Our study had some limitations. First, we did not compare PADRE images with histological findings or amyloid markers, such as PiB-PET. Clinically, direct correlation between MR images and histological findings is unavailable. It has not been validated whether hypointense foci on PADRE coincide with the distribution of PiB-PET. Further comparisons between PADRE and PET imaging are required. In addition, we excluded the basal frontal and medial temporal regions, where the amyloid deposits initially in AD patients, for assessment,[25] because the susceptibility artifacts have sometimes been observed on PADRE in those regions. Second, we could not completely eliminate the hypointense signal attributable to coexisting CAA on PADRE images. In a previous report,[5] both amyloid-containing plaques and CAA showed collocated iron. Aβ deposits in brain parenchyma in AD and in the vascular wall in CAA. However, similar cortical changes have been observed in AD and CAA brain samples.[5] Third, we did not determine the appropriate threshold for all of the cerebral cortices. Therefore, the physiological iron may not be totally excluded in the cortices other than Cn, PrCn, SFG, and STG. However, hypointense foci are predominantly attributable to non-physiologic iron in the specific cortices under the assumption of the double Gaussian model. Further studies are required to determine the appropriate threshold for all cerebral cortices. Fourth, the source of the observed phase differences in PADRE is multifactorial. It is well established that the difference in phase contrast is mainly attributable to iron, and other compounds, such as deoxyhemoglobin, myelin, and proteins, may also contribute.[30] Additionally, the phase is affected by tissue geometry and orientation relative to the main magnetic field (B_0), and phase changes extend beyond altered susceptibility areas.[30] Those factors might have affected the contrast evaluation across the subjects or individual brain regions. To avoid those tissue geometry and orientation factors, 3D-PADRE images may be preferable. Furthermore, our study using 2D-PADRE images lacks quantitative assessment. For objective assessment of all cortices, quantitative studies with 3D-PADRE images are required. Last, our study population was small. Further studies in a larger number of patients with AD and controls are needed to clarify the value of the PADRE technique clinically.

Conclusion

In conclusion, the results of our pilot study suggest the feasibility of PADRE imaging at 3T for differentiation between AD patients and control subjects.

Appendix

Aβ in the human cortex of AD patients associates with several types of iron originating from heme iron and non-heme iron including ferritin representing negative phase value, because those types of iron have a positive susceptibility relative to water molecules. The other important source for the negative phase in the cerebral cortices is non-heme iron due to aging. Although Aβ-related iron includes both heme- and non-heme iron, the susceptibility of heme-iron in Aβ dominantly affects on the phase information. Therefore, it was reasonably assumed that the phase distribution was factorized into corresponding two Gaussian distributions.

For random process corresponding to iron accumulation due to aging, Lathi and Ding[31] had shown it should be Gaussian distribution if signal-to-noise ratio is high enough (>3). Although the phase of Aβ related iron in the local region may show non-Gaussian distribution, the sum of those phase is predicted to be Gaussian distribution based on the central limit theorem.[32]

These are summarized as follows:

I. Iron in the brain cortex consists of Aβ- and age-related iron.
II. Phase distribution of the two types of iron accumulation forms Gaussian.

We may fit phase distribution in the cortex with the sum of two Gaussians by above assumptions,

$$\text{(A.1)} \quad D(\theta) = A_1\, e^{-a_1(\theta-b_1)^2} + A_2\, e^{-a_2(\theta-b_2)^2}$$

where $D(\theta)$ is a phase distribution in the cortex, $A_1\, e^{-a_1(\theta-b_1)^2}$ is a Gaussian distribution representing iron accumulation due to aging with real parameters, A_1, a_1 and b_1, and $A_2\, e^{-a_2(\theta-b_2)^2}$ is a Gaussian distribution representing iron in the Aβ with real parameters A_2, a_2 and b_2 (Fig. 7). Because the number of phases of age-related iron should be dominating

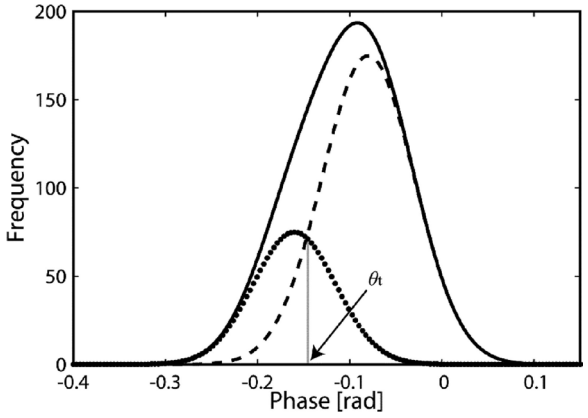

Fig. 7 A model figure of two Gaussian fit in the phase value histogram. The horizontal axis indicates the phase value, and the vertical axis indicates the frequency (number of counts) at each phase value. Phase data (solid line) is fitted by two Gaussians; age-related iron (dashed line) and iron in the Aβ (dotted line). The intersection (θ_t) was numerically derived by fitted parameters. In this model, we set parameters as, $A_1 = 175$, $a_1 = 200$ [1/rad], $b_1 = -0.08$ [rad], $A_2 = 75$, $a_1 = 250$ [1/rad] and $b_1 = -0.16$ [rad] resulting in $\theta_t = -0.142$ [rad]. In this case, phase difference enhanced (PADRE) would select phase band below than θ_t to enhance Aβ. rad, radian.

component of total distribution, the center of mass of first distribution b_1 is to be located around peak of total phase distribution. Therefore, phase of iron in the Aβ is dominant in lower than intersection of two Gaussian distribution defined by, $\theta_t = -(\alpha + \sqrt{\alpha^2 - \beta\gamma}) / \beta$, where $\alpha = a_1 b_1 - a_2 b_2$, $\beta = a_1 - a_2$ and $\gamma = a_1 b_1^2 - a_2 b_2^2 - \ln \frac{A_1}{A_2}$. PADRE selects phase lower than θ_t and enhances it to show Aβ on the PADRE image as hypointense signals. In this study, we defined the threshold θ_t by applying two Gaussians model to data of AD patients and applied it both of AD patients and control subjects. It is rationally expected that number of enhanced PADRE signals of AD patients is to be higher than that of controls since area between two Gaussians lower than θ_t, which may represent number of Aβ, is higher than that of controls.

Conflicts of Interest

T. Yoneda received a research grant from Philips Healthcare. M. Tateishi, M. Kitajima, T. Hirai, M. Hashimoto, N. Kurehana, H. Uetani, R. Fukuhara, M. Azuma, and Y. Yamashita have no conflicts of interest.

References

1. Nelson PT, Braak H, Markesbery WR. Neuropathology and cognitive impairment in Alzheimer disease: a complex but coherent relationship. J Neuropathol Exp Neurol 2009; 68:1–14.
2. Ikonomovic MD, Klunk WE, Abrahamson EE, et al. Post-mortem correlates of in vivo PiB-PET amyloid imaging in a typical case of Alzheimer's disease. Brain 2008; 131:1630–1645.
3. Klunk WE, Engler H, Nordberg A, et al. Imaging brain amyloid in Alzheimer's disease with pittsburgh compound-B. Ann Neurol 2004; 55:306–319.
4. Rowe CC, Ng S, Ackermann U, Gong SJ, et al. Imaging beta-amyloid burden in aging and dementia. Neurology 2007; 68:1718–1725.
5. van Rooden S, Maat-Schieman ML, Nabuurs RJ, et al. Cerebral amyloidosis: postmortem detection with human 7.0-T MR imaging system. Radiology 2009; 253:788–796.
6. van Rooden S, Doan NT, Versluis MJ, et al. 7T T_2^*-weighted magnetic resonance imaging reveals cortical phase differences between early- and late-onset Alzheimer's disease. Neurobiol Aging 2015; 36:20–26.
7. Mittal S, Wu Z, Neelavalli J, Haacke EM. Susceptibility-weighted imaging: technical aspects and clinical applications, part 2. AJNR Am J Neuroradiol 2009; 30:232–252.
8. Haacke EM, Liu S, Buch S, Zheng W, Wu D, Ye Y. Quantitative susceptibility mapping: current status and future directions. Magn Reson Imaging 2015; 33:1–25.
9. Ide S, Kakeda S, Korogi Y, et al. Delineation of optic radiation and stria of Gennari on high-resolution phase difference enhanced imaging. Acad Radiol 2012; 19: 1283–1289.
10. Kakeda S, Korogi Y, Yoneda T, et al. A novel tract imaging technique of the brainstem using phase difference enhanced imaging: normal anatomy and initial experience in multiple system atrophy. Eur Radiol 2011; 21: 2202–2210.
11. Kitajima M, Hirai T, Yoneda T, et al. Visualization of the medial and lateral geniculate nucleus on phase difference enhanced imaging. AJNR Am J Neuroradiol 2015; 36: 1669–1674.
12. Yoneda T, Hashimoto K, Kuniyasu A, et al. Statistical phase noise elimination for amyloid plaque detection. In: Proceedings of the 23rd Annual Meeting of ISMRM, Toronto, 2015, 2223.
13. McKhann G, Drachman D, Folstein M, Katzman R, Price D, Stadlan EM. Clinical diagnosis of Alzheimer's disease: report of the NINCDS-ADRDA work group under the auspices of department of health and human services task force on Alzheimer's disease. Neurology 1984; 34:939–944.
14. Vanhoutte G, Dewachter I, Borghgraef P, Van Leuven F, Van der Linden A. Noninvasive in vivo MRI detection of neuritic plaques associated with iron in APP[V717I] transgenic mice, a model for Alzheimer's disease. Magn Reson Med 2005; 53:607–613.
15. Benveniste H, Einstein G, Kim KR, Hulette C, Johnson GA. Detection of neuritic plaques in Alzheimer's disease by magnetic resonance microscopy. Proc Natl Acad Sci USA 1999; 96:14079–14084.
16. Nakada T, Matsuzawa H, Igarashi H, Fujii Y, Kwee IL. In vivo visualization of senile-plaque-like pathology in Alzheimer's disease patients by MR microscopy on a 7T system. J Neuroimaging 2008; 18:125–129.
17. Helpern JA, Lee SP, Falangola MF, et al. MRI assessment of neuropathology in a transgenic mouse model of Alzheimer's disease. Magn Reson Med 2004; 51:794–798.
18. Connor JR, Snyder BS, Beard JL, Fine RE, Mufson EJ. Regional distribution of iron and iron-regulatory proteins in the brain in aging and Alzheimer's disease. J Neurosci Res 1992; 31:327–335.
19. Wegiel J, Wang KC, Imaki H, et al. The role of microglial cells and astrocytes in fibrillar plaque evolution in transgenic APP(SW) mice. Neurobiol Aging 2001; 22:49–61.
20. Mehlhase J, Gieche J, Widmer R, Grune T. Ferritin levels in microglia depend upon activation: modulation by reactive oxygen species. Biochim Biophys Acta 2006; 1763:854–859.
21. Mandrekar-Colucci S, Landreth GE. Microglia and inflammation in Alzheimer's disease. CNS Neurol Disord Drug Targets 2010; 9:156–167.
22. Hallgren B, Sourander P. The effect of age on the non-haemin iron in the human brain. J Nurochem 1958;3: 41–51.
23. Oyama R, Yamamoto H, Titani K. Glutamine synthetase, hemoglobin alpha-chain, and macrophage migration inhibitory factor binding to amyloid beta-protein: their identification in rat brain by a novel affinity chromatography and in Alzheimer's disease brain by immunoprecipitation. Biochim Biophys Acta 2000; 1479:91–102.

24. Wu CW, Liao PC, Yu L, Corey-Bloom J. Hemoglobin promotes Abeta oligomer formation and localizes in neurons and amyloid deposits. Neurobiol Dis 2004; 17:367–377.
25. Petrella JR. Neuroimaging and the search for a cure for Alzheimer disease. Radiology 2013; 269:671–691.
26. Marcus C, Mena E, Subramaniam RM. Brain PET in the diagnosis of Alzhemier's disease. Clin Nucl Med 2014; 39:e413–e426.
27. Arnold SE, Hyman BT, Flory J, Damasio AR, Van Hoesen GW. The topographical and neuroanatomical distribution of neurofibrillary tangles and neuritic plaques in the cerebral cortex of patients with Alzheimer's disease. Cereb Cortex 1991; 1:103–116.
28. Tiraboschi P, Hansen LA, Thal LJ, Corey-Bloom J. The importance of neuritic plaques and tangles to the development and evolution of AD. Neurology 2004; 62:1984–1989.
29. Villemagne VL, Burnham S, Bourgeat P, et al; Australian Imaging Biomarkers and Lifestyle (AIBL) Research Group. Amyloid β deposition, neurodegeneration, and cognitive decline in sporadic Alzheimer's disease: a prospective cohort study. Lancet Neurol 2013; 12:357–367.
30. Yao B, Li TQ, Gelderen Pv, Shmueli K, de Zwart JA, Duyn JH. Susceptibility contrast in high field MRI of human brain as a function of tissue iron content. Neuroimage 2009; 44: 1259–1266.
31. Lathi BP, Ding Z. Sinusoidal Signl in Noise, In: Adel S. Sedra ed. Modern digital and analog communication systems. International 4th ed. New York, Oxford University Press, 2009;498–499.
32. Kampen NGv. The central limit theorem, In: Stochastic processes in physics and chemistry. 2nd ed. Amsterdam, the Netherlands, Elsevier, 1992;26–29.